Nonlinear Dyn (2016) 84:237–249
DOI 10.1007/s11071-015-2442-1

ORIGINAL PAPER

Nonlinear dynamics modeling and performance prediction for underactuated AUV with fins

Xiao Liang · Ye Li · Zhouhua Peng · Jundong Zhang

Received: 12 September 2015 / Accepted: 23 September 2015 / Published online: 29 October 2015

Abstract The application of autonomous underwater vehicles (AUV) is widespread with the development of the activities in deep ocean. For low energy consumption, low resistance and excellent maneuverability, fins are usually used to modify AUV hydrodynamic forces. The underactuated AUV can do gyratory motion by vertical fins and do diving and rising motion by horizontal fins. However, the modeling and performance prediction for the underactuated AUV with fins have not been solved well. We build the dynamics and kinematics model in 6-DOF for the underactuated AUV with fins and analyze the forces and hydrodynamic coefficients in detail, especially the fin effect. Various hull hydrodynamic coefficients are obtained by CFD numerical computation. A series of simulation experiments are conducted to predict AUV hydrodynamic performance, and the feasibility and accuracy are verified by comparing the results on WL-II underactuated AUV in ocean experiments.

X. Liang (✉)
College of Traffic Equipment and Ocean Engineering, Dalian Maritime University, Dalian, China
e-mail: liangxiao687@sina.com; liangxiao19801012@126.com

Y. Li
National Key Laboratory of Autonomous Underwater Vehicle Technology, Harbin Engineering University, Harbin, China

Z. Peng · J. Zhang
College of Marine Engineering, Dalian Maritime University, Dalian, China

Keywords Underactuated AUV · Dynamics modeling · Performance prediction · Fins · CFD numerical computation

1 Introduction

With the development of the activities in deep ocean, application of the autonomous underwater vehicles (AUV) is widespread, and there is a very prominent prospect. The research on the AUV includes many areas, such as vehicle (carrier/platform) design, architecture, motion control, intelligent planning and decision making [1–5]. Researchers dedicate themselves to improving the performance on modularization, low-cost AUV in such applications as long-range oceanographic survey, autonomous docking and shallow-water mine countermeasures. These goals can be achieved through the improvement of maneuvering precision and motion control capability with energy constraints. For low energy consumption, low resistance and excellent maneuverability, fins are usually used to modify AUV hydrodynamic force. The underactuated AUV with fins can do gyratory motion by vertical fins and do diving and rising motion by horizontal fins. Therefore, the control system of the propeller-fin-drived AUV is very different to the conventional only-propeller-drived AUV.

A mathematic model for the underactuated AUV with fins based on a combination of theory and empirical data would provide an efficient platform for con-

trol system development, and an alternative to the typical trial-and-error method of control system tuning. Although some modeling and simulation methods have been proposed and applied [6–12], there is no standard procedure for modeling the underactuated AUV with fins in industry. Therefore, the modeling and simulation of the underactuated AUV is a challenge.

This paper describes the development and verification of a 6-DOF nonlinear model for the underactuated AUV with fins. In the model, the external force and moment resulting from hydrostatics, hydrodynamic lift and drag, added mass, and the thrusters and fins are all analyzed and expressed in matrix form. The equations describing the rigid-body dynamics are left in nonlinear form to better simulate the AUV inherently nonlinear behavior. Through CFD numerical computation, we simulate the PMM in circulating tank and obtain main hydrodynamic coefficients and calculate the lift and drag curves of fins [13,14]. Moreover, considering the influence of current motion [15], motion simulation is achieved through numeric integration of the motion equations.

A series of motion simulation are conducted, and data are compared with dynamics data collected in ocean experiments. The comparison results show that the nonlinear model gives an accurate estimation to the actual motion of the AUV. The research object is WL-II mini-AUV, which is a small, low-cost platform serving in a range of oceanographic applications [16,17].

2 Dynamics and kinematics modeling for underactuated AUV with fins

2.1 Coordinate system and motion parameters definition

The research object of this paper is WL-II AUV, which is a mini-underactuated AUV with fins developed by Harbin Engineering University, China. WL-II AUV belongs to a propeller-fin-drived AUV, and the velocity can reach 5 kn in design and 8 kn in maximum. In the paper, the simplified model is shown in Fig. 1.

It is convenient to analyze the equations of the rigid-body motion respecting to a body-fixed reference frame which keep the body geometry invariant all the time. Basing on the recommendation of International Towing Tank Conference (ITTC) and the Society of Naval Architects and Marine Engineers (SNAME), we build

Fig. 1 Simplified model of WL-II AUV

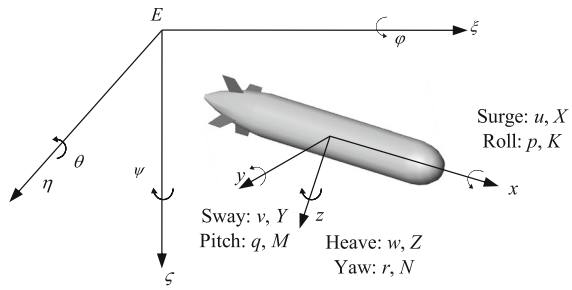

Fig. 2 Global coordinates and local coordinates systemV

two reference coordinates [18]. Start with the application of Newton II law to the AUV motion by a fixed inertial frame of reference (global coordinates), and then transfer the equations to the body-fixed coordinates (local coordinates) through coordinate transformation relation. We can obtain 6-DOF equations of the rigid-body motion referred to as surge, sway, heave, roll, pitch and yaw. The global coordinates and local coordinates are illustrated in Fig. 2.

Considering shape characteristics for most AUVs, the mathematic model is basing on the hypothesis that the AUV is symmetric on the xoz plane. Defining generalized position vector, generalized velocity vector and generalized force vector, the motion vector includes

1. Position and attitude, in $E-\xi\eta\zeta$

$$R = \left[r \ \Lambda \right]^{\mathrm{T}} r = \left[\xi \ \eta \ \zeta \right]^{\mathrm{T}} \Lambda = \left[\varphi \ \theta \ \psi \right]^{\mathrm{T}}$$

2. Linear and angular velocities, in o-xyz

$$V = \left[U^{\mathrm{T}} \ \Omega^{\mathrm{T}} \right]^{\mathrm{T}} U = \left[u \ v \ w \right]^{\mathrm{T}} \Omega = \left[p \ q \ r \right]^{\mathrm{T}}$$

3. Force and moment parameters, in o-xyz

$$\tau = \left[F^{\mathrm{T}} \ M^{\mathrm{T}} \right]^{\mathrm{T}} F = \left[X \ Y \ Z \right]^{\mathrm{T}} M = \left[K \ M \ N \right]^{\mathrm{T}}$$

2.2 Dynamics model

Basing on momentum theorem, the AUV dynamic equation is

$$M_{RB}\dot{V} + C_{RB}(V)V = \tau \tag{1}$$

where M_{BR} is the generalized mass matrix of the vehicle body, and $C_{RB}(V)$ is the Coriolis and centripetal force matrix. M_{BR} is given by

$$M_{BR} = \begin{bmatrix} m & 0 & 0 & 0 & mz_{\mathrm{G}} & -my_{\mathrm{G}} \\ 0 & m & 0 & -mz_{\mathrm{G}} & 0 & mx_{\mathrm{G}} \\ 0 & 0 & m & my_{\mathrm{G}} & -mx_{\mathrm{G}} & 0 \\ 0 & -mz_{\mathrm{G}} & my_{\mathrm{G}} & J_x & J_{xy} & J_{xz} \\ mz_{\mathrm{G}} & 0 & -mx_{\mathrm{G}}J_{yx} & J_y & J_{yz} & \\ -my_{\mathrm{G}} & mx_{\mathrm{G}} & 0 & J_{zx} & J_{zy} & J_z \end{bmatrix} \tag{2}$$

where m is the AUV mass, J terms represent the inertial tensors, and x_{G}, y_{G}, z_{G} represent the AUV position barycenter in local coordinates. $C_{RB}(V)$ is given by

$$C_{RB}(V) = \begin{bmatrix} 0 & -mr & mq \\ mr & 0 & -mpr \\ -mq & mp & 0 \\ -m(y_{\mathrm{G}}q + z_{\mathrm{G}}r) & my_{\mathrm{G}}p & mz_{\mathrm{G}}p \\ mx_{\mathrm{G}}u & -m(z_{\mathrm{G}}r + x_{\mathrm{G}}p) & mz_{\mathrm{G}}q \\ mx_{\mathrm{G}}r & my_{\mathrm{G}}r & m(x_{\mathrm{G}}p + y_{\mathrm{G}}q) \end{bmatrix}$$
$$\begin{bmatrix} m(y_{\mathrm{G}}q + z_{\mathrm{G}}r) & -mx_{\mathrm{G}}q & -mx_{\mathrm{G}}r \\ -my_{\mathrm{G}}p & m(z_{\mathrm{G}}r + x_{\mathrm{G}}p) & -my_{\mathrm{G}}r \\ -mz_{\mathrm{G}}p & -mz_{\mathrm{G}}q & m(x_{\mathrm{G}}p + y_{\mathrm{G}}q) \\ 0 & J_{zx}p + J_{zy}q + J_zr & -J_{yx}p - J_yq - J_{yz}r \\ -J_{zx}p - J_{zy}q - J_zr & 0 & J_xp + J_{xy}q + J_{xz}r \\ J_{yx}p + J_yq + J_{yz}r & -J_xp - J_{xy}q - J_{xz}r & 0 \end{bmatrix} \tag{3}$$

Generalized force vector τ at the right of (1) is outside force (or moment) acting on the AUV, including static force vector τ_{G} (gravity and buoyancy), hydrodynamics force vector of the vehicle body (include τ_{A} which is caused by added mass and viscous damping force τ_{V}), and the controlled force vector (include the thruster force τ_{prop} and the fin force τ_{R}). The static force vector τ_{G} reflects the effect of the vehicle weight and buoyancy. The vehicle weight is $W = mg$, and the buoyancy is $B = \rho \bigtriangledown g$, where ρ is the density of the surrounding fluid, and $\bigtriangledown$ is the total volume displaced by the AUV. Therefore, τ_{G} is given by

$$\tau_{\mathrm{G}} = \begin{bmatrix} X_{\mathrm{G}} \\ Y_{\mathrm{G}} \\ Z_{\mathrm{G}} \\ K_{\mathrm{G}} \\ M_{\mathrm{G}} \\ N_{\mathrm{G}} \end{bmatrix} = \begin{bmatrix} -(W-B)\sin\theta \\ (W-B)\sin(j)\cos\theta \\ (W-B)\cos(j)\cos\theta \\ y_{\mathrm{G}}W - y_BB\cos(j)\cos\theta - (z_{\mathrm{G}}W - z_BB)\sin(j)\cos\theta \\ -x_{\mathrm{G}}W - x_BB\cos(j)\cos\theta - (z_{\mathrm{G}}W - z_BB)\sin\theta \\ x_{\mathrm{G}}W - x_BB\cos(j)\cos\theta - (y_{\mathrm{G}}W - y_BB)\sin\theta \end{bmatrix} \tag{4}$$

where x_B, y_B, z_B are the vehicle coordinates in body-fixed coordinate system.

τ_{A} which is related to added mass is given by

$$\tau_{\mathrm{A}} = -(M_{\mathrm{A}})\dot{V} + C_{\mathrm{A}}(V)V \tag{5}$$

where is the added mass matrix, which is given by

$$M_{\mathrm{A}} = \begin{bmatrix} \lambda_{11} & 0 & \lambda_{13} & 0 & \lambda_{15} & 0 \\ 0 & \lambda_{22} & 0 & \lambda_{24} & 0 & \lambda_{26} \\ \lambda_{31} & 0 & \lambda_{33} & 0 & \lambda_{35} & 0 \\ 0 & \lambda_{42} & 0 & \lambda_{44} & 0 & \lambda_{46} \\ \lambda_{51} & 0 & \lambda_{53} & 0 & \lambda_{55} & 0 \\ 0 & \lambda_{62} & 0 & \lambda_{64} & 0 & \lambda_{66} \end{bmatrix} \tag{6}$$

where λ terms represent the vehicle added mass.

M_{A} can be also denoted as hydrodynamic coefficients expression:

$$M_{\mathrm{A}} = \begin{bmatrix} X_{\dot{u}} & 0 & X_{\dot{w}} & 0 & X_{\dot{q}} & 0 \\ 0 & Y_{\dot{v}} & 0 & Y_{\dot{p}} & 0 & Y_{\dot{r}} \\ Z_{\dot{u}} & 0 & Z_{\dot{w}} & 0 & Z_{\dot{q}} & 0 \\ 0 & K_{\dot{v}} & 0 & K_{\dot{p}} & 0 & K_{\dot{r}} \\ M_{\dot{u}} & 0 & M_{\dot{w}} & 0 & M_{\dot{q}} & 0 \\ 0 & N_{\dot{v}} & 0 & N_{\dot{p}} & 0 & N_{\dot{r}} \end{bmatrix} \tag{7}$$

$C_{\mathrm{A}}(V)$ is a Coriolis-like matrix induced by M_{A}

$$C_{\mathrm{A}}(V) = \begin{bmatrix} 0 & 0 & 0 & 0 & a_3 & -a_2 \\ 0 & 0 & 0 & -a_3 & 0 & a_1 \\ 0 & 0 & 0 & a_2 & -a_1 & 0 \\ 0 & a_3 & -a_2 & 0 & b_3 & -b_2 \\ -a_3 & 0 & a_1 & -b_3 & 0 & b_1 \\ a_2 & -a_1 & 0 & b_2 & -b_1 & 0 \end{bmatrix} \tag{8}$$

where

$$\begin{cases} a_1 = \lambda_1 1u + \lambda_1 3w + \lambda_1 5q \\ a_2 = \lambda_2 2v + \lambda_2 4p + \lambda_2 6r \\ a_3 = \lambda_3 1u + \lambda_3 3w + \lambda_3 5q \\ b_1 = \lambda_4 2v + \lambda_4 4p + \lambda_4 6r \\ b_2 = \lambda_5 1u + \lambda_5 3w + \lambda_5 5q \\ b_3 = \lambda_6 2v + \lambda_6 4 + \lambda_4 6r \end{cases}$$

The viscous damping force is given by

$$\tau_{\mathrm{V}} = D(V)V \tag{9}$$

The damping matrix $D(V)$ is given by

$$D(V) = \begin{bmatrix} X_u + X_{u|u|}|u| & 0 & 0 \\ 0 & Y_v + Y_{v|v|}|v| & 0 \\ Z_0|u| & 0 & Z_w + Z_{w|w|}|w| \\ 0 & 0 & 0 \\ M_0|u| & 0 & 0 \\ 0 & 0 & 0 \end{bmatrix} \begin{bmatrix} 0 & 0 & 0 \\ 0 & 0 & 0 \\ 0 & 0 & 0 \\ K_p + K_{p|p|}|p| & 0 & 0 \\ 0 & M_q + M_{q|q|}|q| & 0 \\ 0 & 0 & N_r + N_{r|r|}|r| \end{bmatrix} \tag{10}$$

where X_u, Y_v, Z_w, K_p, M_q and N_r are the linear damping coefficients. $Y_{v|v|}$, $Z_{w|w|}$, $K_{p|p|}$, $M_{q|q|}$, $X_{u|u|}$ and $N_{r|r|}$ are the quadratic damping coefficients. M_0 and Z_0 are the effect caused by the dissymmetry on xoy plane.

The external force and moment vector produced by thrusters are defined as

$$\tau = LT_{\mathrm{prop}} \tag{11}$$

where L is a mapping matrix, and T_{prop} is the thrust vector produced by thrusters given by

$$T_{\mathrm{prop}} = \begin{bmatrix} T_1 \\ T_2 \\ \vdots \\ T_n \end{bmatrix} \tag{12}$$

T_{prop} is to find the overall force and moment acting on the vehicle.

Hydrodynamics of a single thruster is usually obtained through the in-water test. A series of advance coefficient J corresponding to the thrust coefficient K_T data can be obtained from the in-water test. Data from an in tank test are shown in Fig. 3. We fit the curve by least squares and obtain the fitted $J - K_T$ curve. In practical applications, we obtain advance coefficient J and substitute it into fitted $J - K_T$ curve to obtain K_T. Finally, the thrust can be obtained. Detailed process is as follows:

1. We obtain the advance coefficient from fluid velocity cross the propeller, the propeller diameter D, and the screw propeller rotate speed n (n is determined by controller): $J = \frac{V_{\mathrm{prop}}}{nD}$.
2. We put J into fitted $J - K_T$ curve to obtain force coefficient K_T.
3. We obtain the thrust forces by $T = K_T n_2 D_4$.

The overall external force and moment vector produced by fins τ are given by

$$\tau_{\mathrm{R}} = \begin{bmatrix} X_{\mathrm{R}} \\ Y_{\mathrm{R}} \\ Z_{\mathrm{R}} \\ K_{\mathrm{R}} \\ M_{\mathrm{R}} \\ N_{\mathrm{R}} \end{bmatrix} \tag{13}$$

According to every single fin force and the installation position, τ can be obtained.

As to a control fin on the vehicle, the hydrodynamic force can be decomposed into two directions: lift force

L vertical to stream current and drag force D along stream current. Lift force and drag force can be calculated by the following equations:

$$\begin{cases} L = \frac{1}{2} C_{\mathrm{L}} \rho A_{\mathrm{R}} v_g^2 \\ D = \frac{1}{2} C_{\mathrm{D}} \rho A_{\mathrm{R}} v_g^2 \end{cases} \tag{14}$$

where C_{L} is the fin lift coefficient, C_{D} is the fin drag coefficient, $A_c calculated by the following equations$ is the fin platform area, and v_e is the effective fin velocity. The values of lift coefficient C_{A} and drag coefficient C_{D} are related to effective fin angle of attack α (Fig. 4).

We can tank experiments, CFD computation or empirical formula to obtain C_{L} andC_{D}. Each methods are discussed as follows.

1) A series of data of angles of attack α vs. lift coefficient C_{L} and drag coefficient C_{D} can be obtained from hydrodynamic experiments on WL-II AUV, and then, fitted curves of C_{L} and C_{D} can be generated through least squares fit. The fitted curves of a fin are shown in Fig. 3. When we know the current angle of attack of fin on the AUV, the values of C_{L} and C_{D} under this angle can be obtained by curves interpolation.
   The effective fin angles of attack are given by
2) We also can use CFD method to predict the fin performance, and the results are shown in Fig. 5.
3) The empirical equations to calculate are given by

$$C_{\mathrm{L}} = \frac{\partial C_{\mathrm{L}}}{\partial \alpha} \times \alpha + \frac{C_{\mathrm{DC}}}{\lambda} (\alpha 57.3)^2 \tag{15}$$

$$\frac{\partial C_{\mathrm{L}}}{\partial \alpha} = \frac{0.9(2\pi)\lambda}{57.3\left[\cos \Lambda \sqrt[2]{\frac{\lambda^2}{\cos^4 \Lambda}} + 1.8\right]} \tag{16}$$

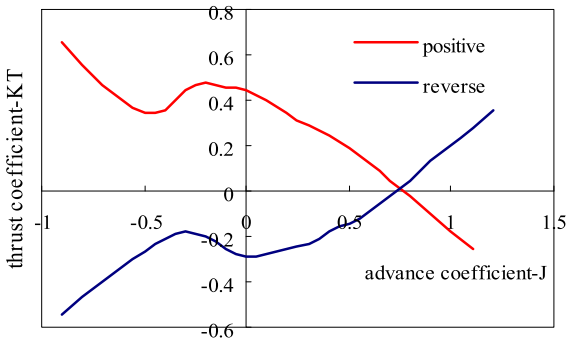

Fig. 3 Capability curves of thrusters

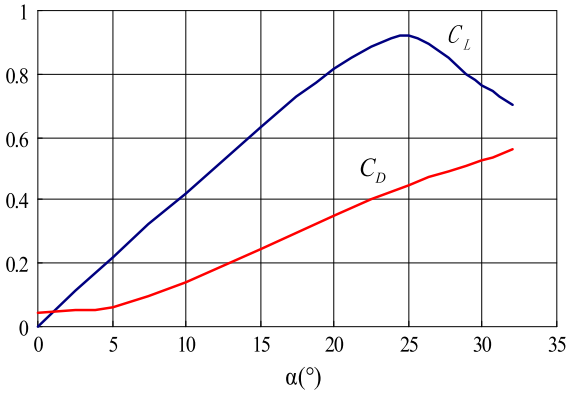

Fig. 4 Lift and drag coefficient curves

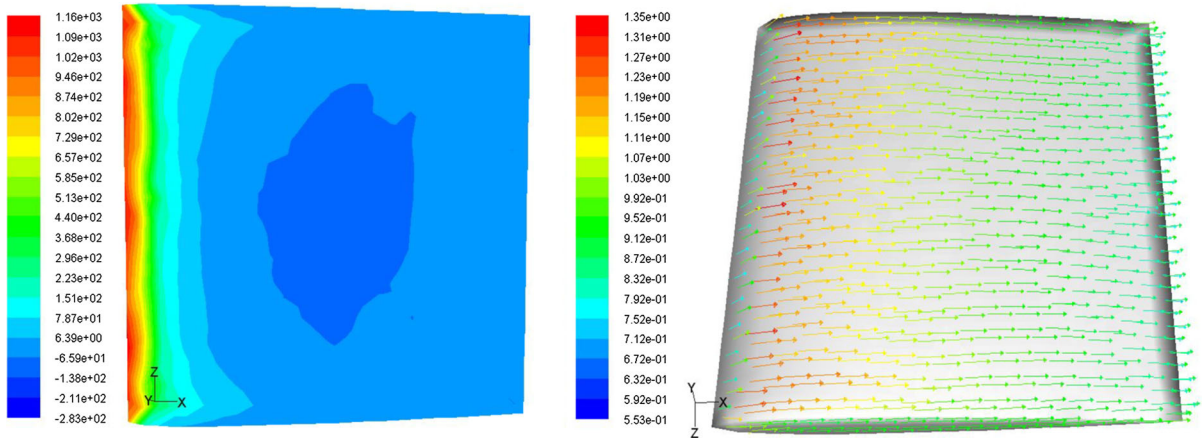

Fig. 5 Pressure distribution and fluid velocity vector

$$C_{\mathrm{D}} = C_{d0} + \frac{C_{\mathrm{L}}^2}{e\pi\lambda} \tag{17}$$

where $\frac{\partial C_{\mathrm{L}}}{\partial \alpha}$ is the slope at=0 in lift coefficient curves, and C_{DC} is the drag coefficient of cross-current which depends on tip shape and rake ratio (e.g., quadrate tip: $C_{\mathrm{DC}} = 0.8$. Smooth tip: $C_{\mathrm{DC}} = 0.4$). C_{d0} is the airfoil profile drag coefficient (viscous drag). For the profile section NACA0015, $C_{d0} = 0.0065$. Λ is the sweptback angle at 1/4 chord of the fin. λ is the aspect ratio. α is the angle of attack (degree).

In order to obtain C_{L} and C_{D}, we should know the real effective angle of attack [19,20]. As the fin located at some offset from the origin of the AUV coordinate system, it experiences the following effective velocities

$$\begin{cases} u_{\mathrm{fin}} = u + z_{\mathrm{fin}} - y_{\mathrm{fin}} r \\ v_{\mathrm{fin}} = v + x_{\mathrm{fin}} r - z_{\mathrm{fin}} p \\ w_{\mathrm{fin}} = w + y_{\mathrm{fin}} - x_{\mathrm{fin}} q \end{cases} \tag{18}$$

where x_{fin}, y_{fin} and z_{fin} are the body-fixed coordinates of the fin posts.

The effective fin angles of attack δ_{se} and δ_{re} are given by

$$\begin{cases} \delta_{se} = \delta_s + \beta_{se} \\ \delta_{re} = \delta_r + \beta_{re} \end{cases} \tag{19}$$

where δ_r and δ_s are the fin angles referenced to the vehicle hull, β_{re} and β_{se} are the effective angles of attack of the fin zero plane, as shown in Fig. 4 (Fig. 6). β_{re} and β_{se} are given by

$$\begin{cases} \beta_{re} = \frac{v_{\mathrm{fin}}}{u_{\mathrm{fin}}} = \frac{v + x_{\mathrm{fin}} r - z_{\mathrm{fin}} p}{u + z_{\mathrm{fin}} - y_{\mathrm{fin}} r} \\ \beta_{se} = \frac{w_{\mathrm{fin}}}{u_{\mathrm{fin}}} = \frac{w + y_{\mathrm{fin}} - x_{\mathrm{fin}} q}{u + z_{\mathrm{fin}} - y_{\mathrm{fin}} r} \end{cases} \tag{20}$$

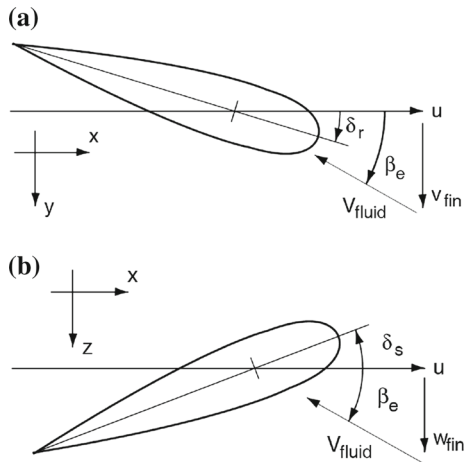

Fig. 6 Pressure distribution and fluid velocity vector. **a** Effective fin angle of attack, **b** effective stern plane angle of attack

2.3 Kinematics model

The coordinate transformation between body-fixed coordinate system and inertial coordinate system is given by

$$\begin{bmatrix} \dot{\xi}_{\mathrm{G}} \\ \dot{\eta}_{\mathrm{G}} \\ \dot{\zeta}_{\mathrm{G}} \\ \dot{\varphi} \\ \dot{\theta} \\ \dot{\psi} \end{bmatrix} = \begin{bmatrix} T_1 & 0_3 \\ 0_3 & T_2 \end{bmatrix} \begin{bmatrix} u \\ v \\ w \\ p \\ q \\ r \end{bmatrix} \tag{22}$$

where ξ_{G}, η_{G} and ζ_{G} are the barycentre coordinates in inertial coordinate system, T_1 and T_2 are coordinate transform matrix given by

$$T_1 = \begin{bmatrix} \cos\psi\cos\theta & \cos\psi\sin\theta\sin\varphi - \sin\psi\cos\varphi & \cos\psi\sin\theta\cos\varphi + \sin\psi\sin\varphi \\ \sin\psi\cos\theta & \sin\psi\sin\theta\sin\varphi + \cos\psi\cos\varphi & \sin\psi\sin\theta\cos\varphi - \cos\psi\sin\varphi \\ -\sin\theta & \cos\theta\sin\varphi & \cos\theta\cos\varphi \end{bmatrix} \tag{23}$$

$$T_2 = \begin{bmatrix} 1 & \tan\theta\sin\varphi & \tan\theta\cos\varphi \\ 0 & \cos\varphi & -\sin\varphi \\ 0 & \sin\varphi\sec\theta & \cos\varphi\sec\theta \end{bmatrix} \tag{24}$$

Basing on the above analysis, (1) could be rewritten into more detailed form.

$$M_{RB} + M_{\mathrm{A}}\dot{A} = \tau + \tau_{\mathrm{prop}} + \tau_{\mathrm{R}} + D_{(V)}V - (C_{RB}(V) + C_{\mathrm{A}}(V))V \tag{21}$$

2.4 Numerical integration

Given the complex and highly nonlinear nature of (21) and (22), we will use numerical integration to solve

these equations and obtain the vehicle speed, position and attitude vs time.

The nonlinear state equation of the AUV is given by

$$\dot{x_n} = f(x_n, u_n) \tag{25}$$

where x_n is the state vector, and $u_n$is the input vector:

$$x_n = \left[u \ v \ w \ p \ q \ r \ \xi \ \eta \ \zeta \ \varphi \ \theta \ \psi \right]^{\mathrm{T}} \tag{26}$$

$$u_n = \left[\tau_{\mathrm{prop}} \ \tau_{\mathrm{R}} \right] \tag{27}$$

Here, Runge–Kutta of numerical integration is usually used to solve the equations. Firstly, we calculate the following equations

$$\begin{aligned} k_1 &= x_n + f(x_n, u_n) \\ k_2 &= f(x + \frac{\Delta t}{2} k_1, u_{n+\frac{1}{2}}) \\ k_3 &= f(x + \frac{\Delta t}{2} k_2, u_{n+\frac{1}{2}}) \\ k_4 &= f(x + \Delta t k_4, u_{n+1}) \end{aligned} \tag{28}$$

where the interpolated input vector is

$$u_{n+\frac{1}{2}} = \frac{1}{2}(u_n + u_{n+1}) \tag{29}$$

Then, we combine the above equations

$$x_{n+1} = x_n + \frac{\Delta t}{6}(k_1 + 2k_2 + 2k_3 + k_4) \tag{30}$$

3 Hydrodynamic coefficients acquisition

Hydrodynamic numerical calculations are conducted to obtain inertia and viscous hydrodynamic coefficients. The computational object is the hull model with fins. Numerical calculation is in the both steady and unsteady tank to obtain various hydrodynamic coefficients [15]. Computational grid model is shown in Fig. 7.

3.1 Solving speed coefficients under steady situation

In the steady case, we can solve drag coefficients and horizontal and vertical speed factor.

Drag coefficients Select separate implicit solver and SST k-omega turbulence model widely used. The main initial conditions are selected to the flow velocity and turbulence parameters. The entry speed and resistance for drag coefficients are shown in Table 1.

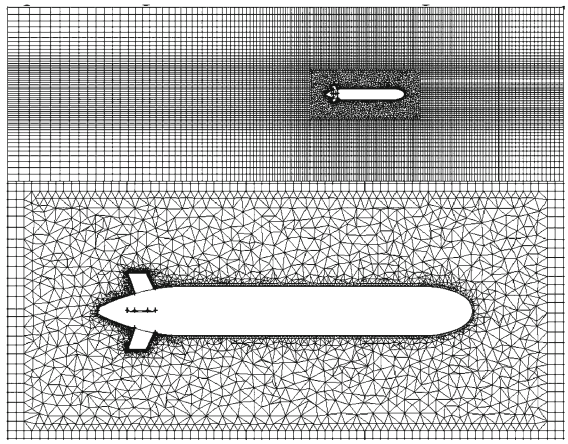

Fig. 7 Mixed grid divide of the AUV as whole/local

Fitting by the method of least squares, and changing to dimensionless, the calculated value of the resistance coefficients is $X'_u u = -0.002563$.

Speed coefficients Speed coefficients are calculated, and in addition to set different velocity inlet, the other settings are the same as the drag coefficients. While setting flow speed $u = 2.5$ m/s, we simulate the models angle of attack changes from 0 to 10 in the control body. Horizontal plane speed coefficient results are shown in Table 2.

Fitting by least squares method, and changing to dimensionless, we obtain vertical and horizontal velocity coefficients:

$$\begin{aligned} Z'_w &= -0.02065, \ M'_w = 0.038809 \\ Y'_v &= -0.07086, \ N'_v = 0.098568 \end{aligned}$$

Table 1 Drag coefficient results

Speed (m/s)	2.0	2.5	4.1
Resistance (N)	−410.5	−626.3	−1590.1
Drag coefficient (10^{-3})	2.65	2.59	2.45

Table 2 Horizontal speed coefficient results

$\beta(\circ)$	3	5	8	10
v (m/s)	0.087	0.218	0.348	0.434
Y (N)	−146	−408.7	−711.4	−1035.2
N($N \cdot m$)	3070	7182.7	11,359.4	13,514.7

3.2 Solving coefficients under unsteady situation

While solving acceleration coefficients and angular acceleration coefficients, we simulate PMM to measure hydrodynamic coefficients by dynamic mesh technology. Model moves in accordance with the law specified in the control domain. At the same time, in order to simulate the infinite flow at the control domain entrance, we set flow speed $u = 2.5$ m/s. According to a different law of motion, the AUV can be divided into pure heave, pure sway, pure pitching and pure shake bow. Considering symmetric characteristics of the AUV, we just need to discuss pure heave and pure pitching motion. Based on each DOF motion equations, we compile user self-defined function (UDF) program and make model hull wall motion in accordance with motion equations in the control domain. Table 3 shows the experimental conditions [21].

While calculation, a motion cycle is divided into 250 time steps. Taking into account the initial subject to oscillation, we calculate five cycles to obtain a stable hydrodynamic graph which changes with time. Based on a stable cycle curve, we use MATLAB to expand the results by Fourier series and fit the corresponding hydrodynamic coefficients. the control body. Horizontal plane speed coefficients results are shown in Table 2 (Table 4).

Because the calculation principles in the case of a steady velocity coefficients are defined by velocity coefficients, so the reliability of velocity coefficients obtained is higher. Eventually, we obtain 17 basic hydrodynamic coefficients in Table 5.

Based on calculation results, we can obtain more high-end and coupled items hydrodynamic coefficients [18] and ultimately meet the simulation.

Table 3 Pure heave and pitch experimental condition table

Heave	Velocity of flow (m/s): 2.5
	Amplitude (a-m): 0.04
	Vibration frequency (Hz): 0.2, 0.4, 0.5
Pitch	Velocity of flow (m/s): 2.5
	Amplitude (θ_0-rad): 1
	Vibration frequency (Hz): 0.2, 0.4, 0.5

Table 4 Vertical plane coefficients by simulation PMM

$Z'_{\dot{w}}$	$M'_{\dot{w}}$	$Z'_{\dot{q}}$	$M'_{\dot{q}}$
−0.00728	−0.00523	−0.00109	0.000126
Z'_{w}	M'_{w}	Z'_{q}	M'_{q}
−0.02065	0.038809	0.002734	0.014233

Table 5 Dimensionless hydrodynamic coefficients

Coefficient	Value	Coefficient	Value
$Z'_{\dot{w}}$	−0.00728	$M'_{\dot{w}}$	−0.00523
Z'_{w}	−0.02065	M'_{w}	0.038809
$Z'_{\dot{q}}$	−0.00109	$M'_{\dot{q}}$	0.000126
Z'_{q}	0.002734	M'_{q}	0.014233
$Y'_{\dot{v}}$	−0.00728	$N'_{\dot{v}}$	−0.00523
Y'_{v}	−0.07086	N'_{v}	0.098568
$Y'_{\dot{r}}$	−0.00109	$N'_{\dot{r}}$	0.000126
Y'_{r}	0.002734	N'_{r}	0.014233
X'_{uu}	−0.00256		

4 Simulation

Based on the above mathematic modeling and analysis, we develop a simulation system and conduct performance prediction for WL-II AUV. We obtain present relative acceleration of the AUV in the global coordinates, and the velocity of next moment through Runge–Kutta numerical integral, and the displacement of next moment further. The operating flowchart is shown in Fig. 8, and the visual simulation system of WL-II AUV is shown in Fig. 9.

4.1 Simulation without disturbance

4.1.1 Simulation of longitudinal motion

First, the AUV navigates in longitudinal straight direction. Given different control instruction, the AUV accelerates from rest state to uniform motion. Figure 10 shows the curves of velocity response. As can be seen, the AUV acceleration time is about 100 s, and the speed responds fast enough, which meet the design requirement that a maximum speed is 8 kn.

4.1.2 Simulation of horizontal rotation motion

Simulation results are given in the case of a pair of vertical fins with the fin angle from 5 to 25. Figure 11

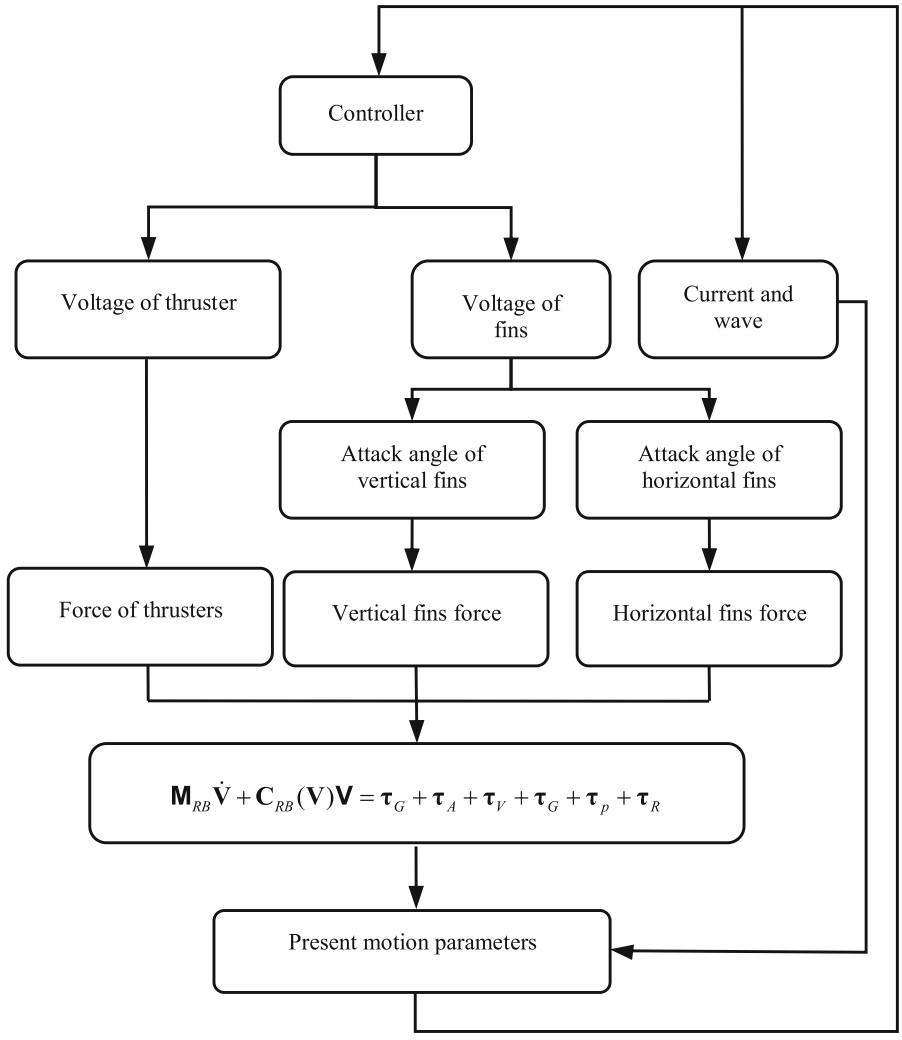

Fig. 8 Operating flowchart of simulation system

shows the trajectory of the AUV gravity center in the horizontal plane. Figure 12 shows the relation curves between rotational diameter and vertical fin angle.

The simulations are conducted under different speeds but the same fin angle. In the chosen speed range, rotational diameter hardly changes with speed, and the minimum rotational diameter is about 65 m.

4.1.3 Horizontal Z-shaped steering motion simulation

Then, we conduct Z-shaped steering motion simulation in the horizontal plane with 0/0 = 10/10, 20/20, by steering a pair of vertical fin simultaneously with 4/s. The results are shown in Fig. 13.

As can be seen, the beyond heading angles are 7.6 and 14.8 corresponding to the 10 and 20 test, and the period is 44 and 61 s. The results suggest that the AUV is of good mobility in the horizontal plane, and the fin has better ability to control heading.

4.1.4 Vertical trapezoidal steering motion simulation

Vertical trapezoidal steering motion simulation descending simulation is conducted by steering the horizontal fins. Longitudinal angle is $\theta_e = 7$, and fin steering rate of fins is 4/s. Fin angle instruction is $\delta_0 = 10$. The results are shown in Fig. 14, and $\zeta(t)$ in the figure is AUV the vertical location.

As can be seen, when the horizontal fin angle turns to zero, the trim angle converges to the initial state due

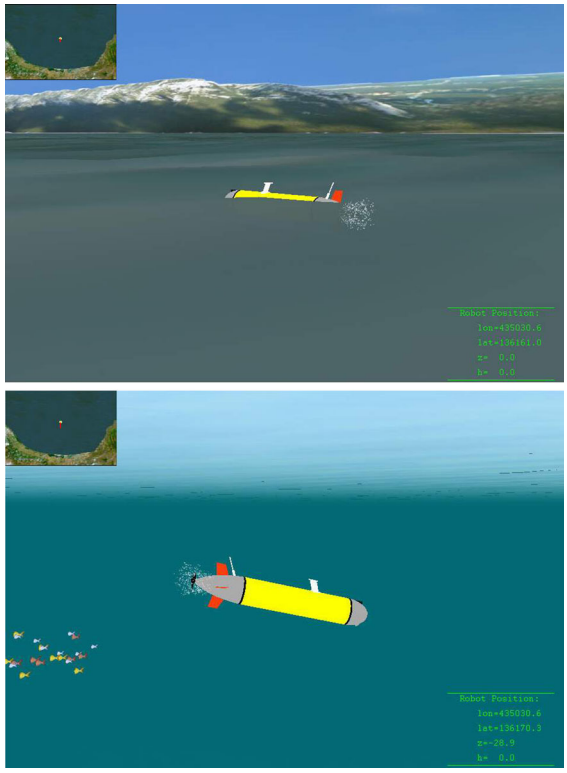

Fig. 9 Visual simulation of WL-II AUV

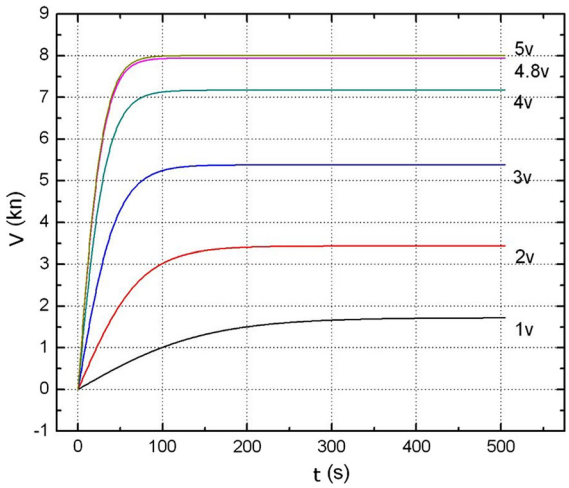

Fig. 10 Curves of longitude velocity response

to its righting moment effect. That is, the AUV has a trim angle caused by an initially interference; however, when the interference disappeared, trim angle has a ability to recover by itself. However, there is no self-recovery capability in depth direction, and it should be corrected via control.

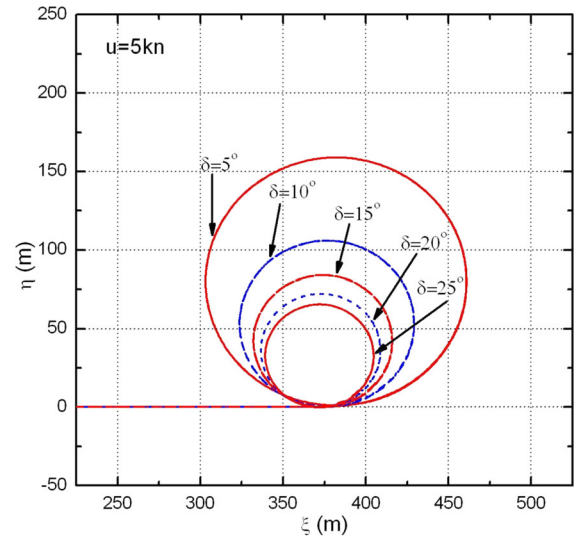

Fig. 11 Horizontal rotary motion simulation

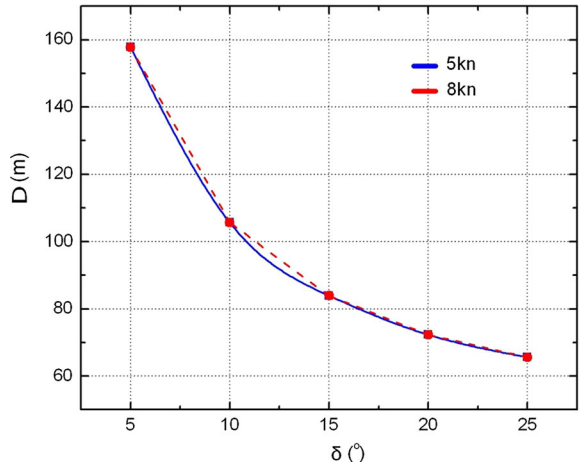

Fig. 12 Relationship between turning radius and fin angle

4.1.5 Space given regular helical motion simulation

Space spiral motion is a rotational descends motion that the AUV makes especially when sailing in a certain depth. The AUV set deep sailing, during which horizontal and vertical fins are rotated to fixed values. It is a coupling of horizontal and vertical motion. Characterization parameters of space steady spiral motion conclude the horizontal projection diameter D_s and liter distance Δ_e. Figure 15 shows the AUV space spiral motion trajectory, with changing the horizontal fin angle to 10 and a vertical fin angle to 5.

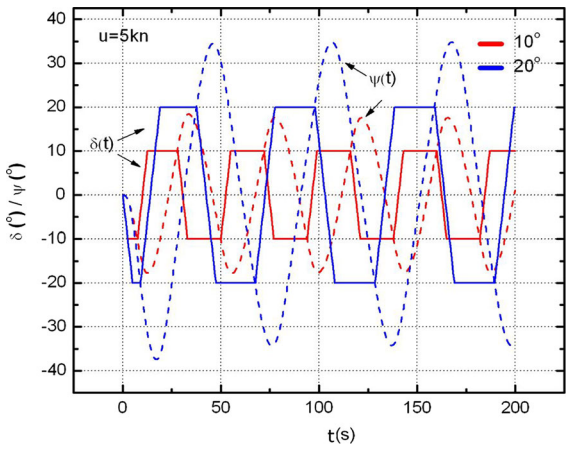

Fig. 13 Curves of fin angle and bow direction angle

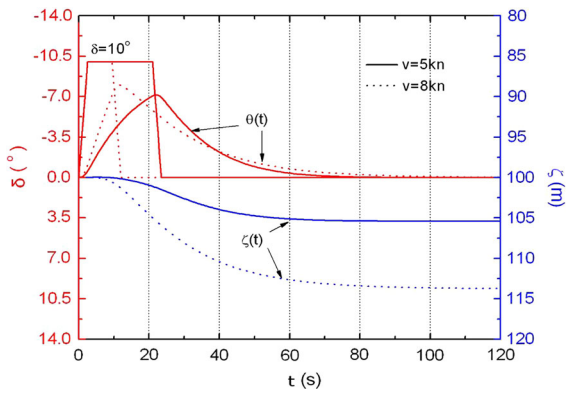

Fig. 14 Vertical trapezoid steering motion simulation

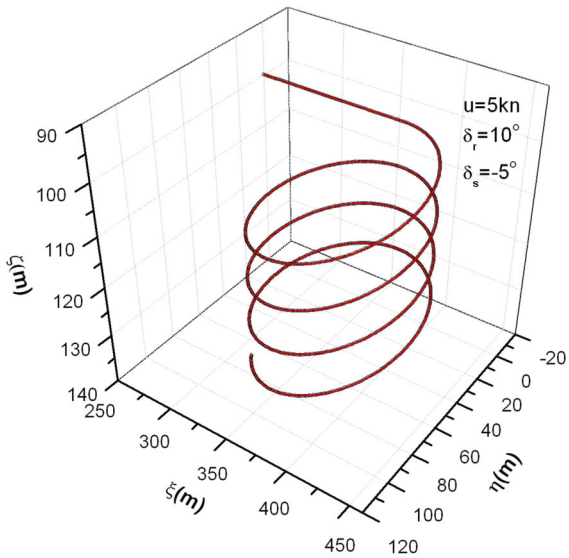

Fig. 15 Space spiral motion trajectory of the AUV

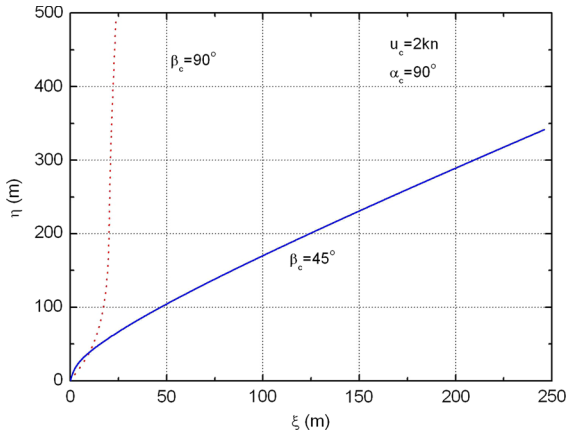

Fig. 16 Trajectory curves under the current

4.2 Simulation under current

Current forces are the essence of current effect on the AUV. Therefore, in the presence of current, the AUV is also affected by the interference current forces in addition to the hull hydrodynamics generated by its motion and actuator thrusts. The essence of the current force is also the hydrodynamics. Therefore, the total forces of the hull hydrodynamics and current disturbance force are directly calculated in this paper.

According to the principle of relative motion and the physical meaning of the hull hydrodynamic coefficients, under the current interference, the hydrodynamics of the AUV are no longer a function of the absolute velocity (u, v, w), but a function of the velocity (u_r, v_r, w_r) relative to the current. As a result, the hull hydrodynamics can be calculated by adopting the AUV velocity relative to the current instead of absolute speed in calm water.

4.2.1 Simulation of longitudinal motion

Figure 16 shows the AUV trajectory curves, in the case of the side flow and inclined side flow angle $c = 90, 45$, the current velocity uc = 2 kn. The AUV itself does not produce thrust, only fluttering freely under the current effect. The results show that the AUV without power will drift along with the current under that condition.

4.2.2 Rotation motion under current disturbance

Figure 17 shows the AUV trajectory curves in the horizontal plane step fin rotation experiment, with $\beta_c = 0$,

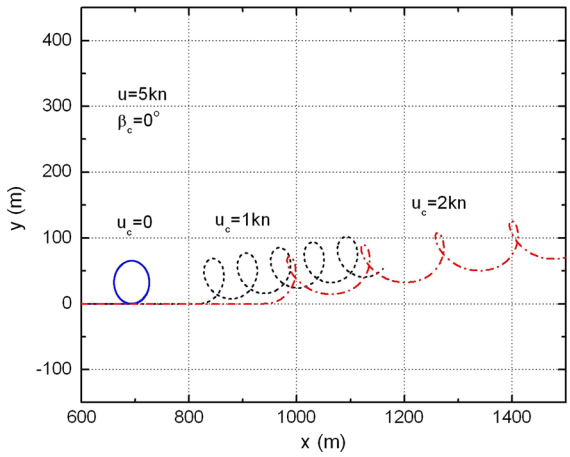

Fig. 17 Cocurrent, rotation trajectory curves

uc = 0, 1, 2 kn. As can be seen, the AUV circles into a spiral trajectory and associated with lateral motion. As a result, in the condition of cocurrent, the effect of current speed and direction on the AUV trajectory must be taken into consideration when the AUV needs to rotate in case of turning around or avoiding collision, and adopting corresponding control measures.

4.2.3 Space spiral motion under current disturbance

Figure 18 shows the AUV trajectory curves of the space motion under current interference, with $c = 90$, $c = 0$, uc = 1 kn. As can be seen, if the current direction is not the same as the AUV sailing direction, horizontal motion will take place when the AUV sinks or rises. It takes special control to do vertical motion strictly. Current should be considered when the AUV needs sink spirally under current environment. To realize AUV steady and accurate sink, in-time control should be employed based on current velocity and direction, compounding the posture and AUV state of motions.

Finally, a part of simulation results are compared with the results of ocean experiments. The zigzag-like motions in horizontal plane and vertical plane are simulated, and the comparisons are shown in Fig. 19. From the comparison between simulation results and experiment results, we can conclude that the nonlinear dynamics model and performance prediction for the underactuated AUV with fins and the numerical integration method are accurate and feasible.

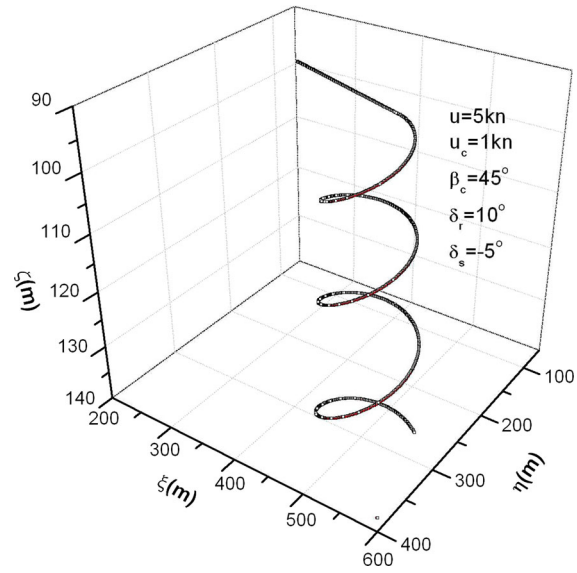

Fig. 18 The curve of the space spiral motion under current

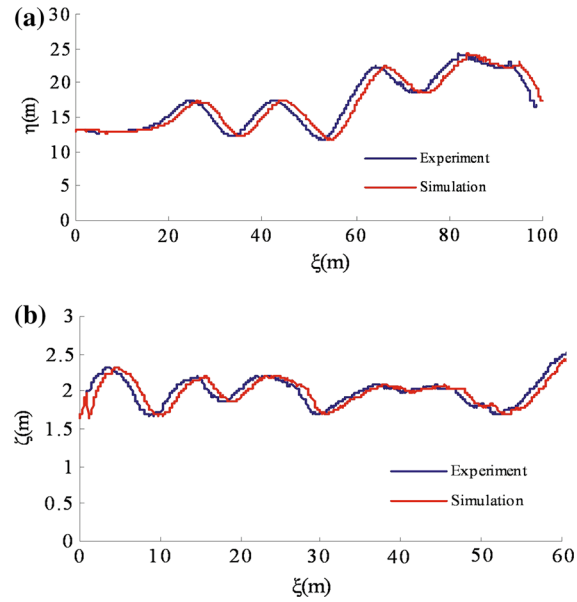

Fig. 19 Comparison between simulations and experiments. **a** Zigzag-like motion in horizontal plane, **b** zigzag-like motion in horizontal plane

5 Conclusion

This paper concentrates on nonlinear dynamics modeling and performance prediction for the underactuated AUV with fins. We build the dynamics and kinematics model in 6-DOF for the underactuated AUV with fins and analyze the forces and hydrodynamic coefficients

in detail, especially the fin effect. Various hull hydrodynamic coefficients are obtained by CFD numerical computation. A series of simulation experiments are conducted to predict AUV hydrodynamic performance. The results verify the feasibility and the superiority of the nonlinear dynamics modeling and performance prediction for the underactuated AUV with fins by comparing the results on WL-II underactuated AUV in ocean experiments. Moreover, the methods and simulation system in this paper also can be used universally to most AUVs.

Acknowledgments This work is supported by the National Natural Science Foundation of China (Grant Nos. 51579022, 51579023, 51209025) and Fundamental Research Funds for the Central Universities of China (Grant Nos. 3132015088, 3132014318).

References

1. Wynn, R.B., Huvenne, V.A.I.: Autonomous underwater vehicles (AUVs): their past, present and future contributions to the advancement of marine geoscience. Mar. Geol. **352**(1), 451–468 (2014)
2. Monique, C.: Autonomous underwater vehicles. Ocean Eng. **36**(1), 1–2 (2009)
3. Xu, Y.R., Pang, Y.J., Gan, Y., Sun, Y.S.: AUV-state-of-the-art and prospect. CAAI Trans. Intell. Syst. **1**(1), 9–16 (2006)
4. Xu, Y.R., Xiao, K.: Technology development of autonomous ocean vehicle. J. Autom. **33**(5), 518–521 (2007)
5. Ke, G.Y., Wu, T., Li, M., Xiao, D.B.: The improvements and trends of the unmanned underwater vehicles. Natl. Def. Sci. Technol. **34**(5), 44–48 (2013)
6. Prestero, T.J.: Development of a six-degree of freedom simulation model for the REMUS autonomous underwater vehicle. In: Proceedings of the OCEANS 2001 MTS/IEEE Conference and Exhibition, pp. 450–455 (2001)
7. Chang, W.J., Liu, J.C., Yu, H.: Mathematic model of the AUV motion control and simulator. Ship Eng. **12**(3), 58–60 (2002)
8. Li, Y., Liu, J.C., Shen, M.: Dynamics model of underwater robot motion control in 6 degrees of freedom. J. Harbin Inst. Technol. **12**(4), 456–459 (2005)
9. Nahon, M.: A simplified dynamics model for autonomous underwater vehicles. J. Ocean Technol. **1**(1), 57–68 (2006)
10. Silva, J., Terra, B., Martins, R., Sousa, J.: Modeling and simulation of the LAUV autonomous underwater vehicle. In: Proceedings of IEEE Conference on Methods and Models in Automation and Robotics, pp. 713–718 (2007)
11. Conte, G., Serrani, A.: Modeling and simulation of underwater vehicles. In: Proceedings of IEEE Symposium on Computer-Aided Control System Design, pp. 62–67 (1996)
12. Timothy, P.: Development of a six-degree of freedom simulation model for the REMUS autonomous underwater vehicle: Oceans. In: MTS/IEEE Conference and Exhibition, pp. 450–455 (2001)
13. Zhang, H., Xu, Y., Cai, H.: Using CFD software to calculate hydrodynamic coefficients. J. Mar. Sci. Appl. **9**, 149–155 (2010)
14. Zhang, H., Pang, Y., Li, Y.: Study of AUV's hydrodynamic coefficients calculation method. J. Wuhan Univ. Technol. (Transp. Sci. Eng.) **35**(1), 15–18 (2011)
15. Wang, Q.: Research on application of variable structure control to AUVs operating in current. A Master Degree Thesis, Harbin Engineering University (2007)
16. Su, Y., Wan, L., Li, Y.: Development of a small autonomous underwater vehicle controlled by thrusters and fins. Robot **29**(2), 151–154 (2007)
17. Wang, B., Su, Y., Qin, Z.: Research on maneuverability and simulation of small autonomous underwater vehicle. J. Syst. Simul. **21**(13), 4149–4158 (2009)
18. Shi, S.: Submarine Maneuverability. National Defence Industry Press, Beijing (1995)
19. Yasser, M.: A new model for the structure of leaves. J. Softw. **6**(4), 662–669 (2011)
20. Li, Y., Liu, J., Xu, Y., Pang, Y.: Dynamics modeling for motion control of underwater vehicle with wing. Robot **27**(2), 128–131 (2005)
21. Li, G., Duan, W.: Experimental study on the hydrodynamic property of a complex submersible. J. Ship Mech. **15**(1), 58–65 (2011)